Chinese Journal of Natural Medicines

Astragali RadixNotoginseng Radix et Rhizoma medicine pair prevents cardiac remodeling by improving mitochondrial dynamic balance

Pingping Lin, Hong Chen, Zekun Cui, Boyang Yu, Junping Kou, Fang Li

Citation: Pingping Lin, Hong Chen, Zekun Cui, Boyang Yu, Junping Kou, Fang Li, Astragali RadixNotoginseng Radix et Rhizoma medicine pair prevents cardiac remodeling by improving mitochondrial dynamic balance, Chinese Journal of Natural Medicines, 2025, 23(1), 54–63. doi: 10.1016/S1875–5364(25)60806–5.

View online: https://doi.org/10.1016/S1875–5364(25)60806–5

Chinese Journal of Natural Medicines 23 (2025) 54-63

Contents lists available at ScienceDirect

Chinese Journal of Natural Medicines

journal homepage: www.cjnmcpu.com/

Original article

Astragali Radix–Notoginseng Radix et Rhizoma medicine pair prevents cardiac remodeling by improving mitochondrial dynamic balance

Pingping Lin, Hong Chen, Zekun Cui, Boyang Yu, Junping Kou, Fang Li*

Jiangsu Key Laboratory of TCM Evaluation and Translational Research, Research Center for Traceability and Standardization of TCMs, School of Traditional Chinese Pharmacy, China Pharmaceutical University, Nanjing 211198, China

ARTICLE INFO

Article history:
Received 11 February 2024
Revised 27 March 2024
Accepted 15 April 2024
Available online 20 January 2025

Keywords:
Astragali Radix–Notoginseng Radix et Rhizoma medicine pair
Mitochondrial dynamics
Transforming growth factor-β1/Smad3 pathway
Cardiac hypertrophy
Cardiac fibrosis

ABSTRACT

Astragali Radix (AR) and Notoginseng Radix et Rhizoma (NR) are frequently employed in cardiovascular disease treatment. However, the efficacy of the AR–NR medicine pair (AN) in improving cardiac remodeling and its underlying mechanism remains unclear. This study aimed to evaluate AN's cardioprotective effect and potential mechanism on cardiac remodeling using transverse aortic constriction (TAC) in mice and angiotensin II (Ang II)-induced neonatal rat cardiomyocytes (NRCMs) and fibroblasts *in vitro*. High-performance liquid chromatography-quadrupole-time of flight tandem mass spectrometry (HPLC-Q-TOF-MS/MS) characterized 23 main components of AN. AN significantly improved cardiac function in the TAC-induced mice. Furthermore, AN considerably reduced the serum levels of *N*-terminal pro-B-type natriuretic peptide (NT-proBNP), cardiac troponin T (CTn-T), and interleukin-6 (IL-6) and mitigated inflammatory cell infiltration. Post-AN treatment, TAC-induced heart size approached normal. AN decreased cardiomyocyte cross-sectional area and attenuated the upregulation of cardiac hypertrophy marker genes (*ANP*, *BNP*, and *MYH7*) *in vivo* and *in vitro*. Concurrently, AN alleviated collagen deposition in TAC-induced mice. AN also reduced the expression of fibrosis-related indicators (COL1A1 and COL3A1) and inhibited the activation of the transforming growth factor-β1 (TGF-β1)/mothers against decapentaplegic homolog 3 (Smad3) pathway. Thus, AN improved TAC-induced cardiac remodeling. Moreover, AN downregulated p-dynamin-related protein (Drp1) (Ser616) expression and upregulated mitogen 2 (MFN-2) and optic atrophy 1 (OPA1) expression *in vivo* and *in vitro*, thereby restoring mitochondrial fusion and fission balance. In conclusion, AN improves cardiac remodeling by regulating mitochondrial dynamic balance, providing experimental data for the rational application of Chinese medicine prescriptions with AN as the main component in clinical practice.

1. Introduction

Heart failure represents the leading cause of mortality worldwide, with its prevalence and fatality rates remaining persistently high [1]. Cardiac remodeling constitutes a common pathological alteration in this context. In response to increased load, the heart and individual cardiomyocytes typically undergo enlargement, progressively developing cardiac hypertrophy and activating pro-fibrotic pathways [2,3]. However, prolonged stress can compromise the heart's systolic function, ultimately leading to heart failure [4]. Therefore, the improvement of early pathological cardiac remodeling is crucial to preventing and treating heart failure.

Mitochondria are the primary source of energy for cellular activities [5]. Mitochondrial dynamics, encompassing fusion and fission processes, regulate mitochondrial number and size [6]. Specifically, optic atrophy 1 (OPA1) and mitogen 2 (MFN-2) govern mitochondrial fusion, while dynamin-related protein (Drp1) controls fission [7]. Research has demonstrated that inhibiting Drp1 mitigates left ventricular hypertrophy and cardiac fibrosis in stress-induced models [8]. Moreover, mice with heart-specific heterozygous deletion of the *Drp1* gene exhibited exacerbated cardiac hypertrophy and mitochondrial dysfunction when subjected to transverse aortic contraction (TAC) [9]. Additionally, the decreased expressions of OPA1 and MFN-2 have been observed in rat models of heart failure and *in vitro* hypertrophic cardiomyocytes [10]. These findings suggest that enhancing mitochondrial homeostasis represents a promising approach for treating cardiac remodeling.

Medicine pairs are two relatively fixed herbs that work synergistically [11]. Astragali Radix (AR), the dried root of *Astragalus membranaceus* (Fisch.) Bge., is known for its Qi-replenishing properties. Previous studies have demonstrated AR's efficacy in reducing apoptosis and improving cardiac function in rats with myocardial ischemia by inhibiting Ca^{2+} influx and activating mitochondrial K_{ATP} channels [12,13]. Additionally, AR has shown the ability to mitigate myocardial oxidative stress damage in rats with viral myocarditis [14]. Notoginseng Radix et Rhizoma (NR), derived

* Corresponding author.
E-mail address: lifangcpu@163.com

https://doi.org/10.1016/S1875-5364(25)60806-5

from the dried roots and rhizomes of *Panax notoginseng* (Burk.) F. H. Chen, is known for invigorating blood and eliminating blood stasis. NR extract has been found to alleviate myocardial ischemia by reducing oxidative stress and inhibiting inflammatory cascades [15, 16]. Furthermore, NR has been reported to induce vascular dilation [17]. The combination of AR and NR has been explored in clinical practice [18] and is widely used for preventing and treating various diseases, including cardiovascular disorders. Several Chinese medicine prescriptions incorporating the AR–NR medicine pair (AN) as a primary component are utilized in cardiovascular treatment, with Qishen Capsule and Qishen Yiqi Dropping Pill being common examples [19]. While numerous studies have reported on the independent effects of AR and NR on cardiovascular disease, the impact of AN on cardiac hypertrophy remains unclear. Moreover, the potential role of AN in improving cardiac remodeling through the modulation of mitochondrial dynamics requires further investigation.

This study investigated the cardioprotective effects of AN on cardiac remodeling in TAC-induced mice *in vivo* and angiotensin II (Ang II)-induced neonatal rat cardiomyocytes (NRCMs) and neonatal rat cardiac fibroblasts (NRCFs) *in vitro*. Furthermore, the research explored the potential mechanisms by which AN improves cardiac remodeling, with a particular focus on the regulation of mitochondrial dynamics. These findings may provide a scientific basis for the use of AN in the prevention and treatment of cardiac remodeling.

2. Materials and methods

2.1. Materials

Astragali Radix was sourced from Yunfu Houde Traditional Chinese Medicine Decoction Pieces Co., Ltd. (Yunfu, China). Notoginseng Radix et Rhizoma was obtained from Sichuan Huotai Pharmaceutical Co., Ltd. (Chengdu, China). Professor Boyang Yu from China Pharmaceutical University identified these herbal medicines. Enalapril (ENP) was procured from Yangtze River Pharmaceutical Group (Nanjing, China). Ang II was acquired from MedChemExpress (NJ, USA). Shanghai Hengyuan Biotechnology Co., Ltd. (Shanghai, China) supplied interleukin-6 (IL-6), *N*-terminal pro-B-type natriuretic peptide (NT-proBNP), and cardiac troponin T (CTn-T) test kits. Bioss antibodies (Beijing, China) provided the Collagen type I alpha 1 (COL1A1) antibody. OriGene Technologies (MD, USA) supplied the Collagen type III alpha 1 (COL3A1) antibody. Abcam (Cambridge, UK) provided anti-transforming growth factor-β1 (TGF-β1), anti-mothers against decapentaplegic homolog 3 (Smad3) and anti-dynamin-related protein 1 (Drp1) primary antibodies. Cell Signal Technology (Boston, USA) supplied anti-p-Smad3 (Ser423/425), anti-MFN-2, anti-OPA1 and anti-p-Drp1 (Ser616). Zen-bioscience (Chengdu, China) provided anti-*β*-actin.

2.2. Decoction preparation

The preparation of AN followed the established clinical ratio of 3∶1 (*W*/*W*), as reported in the literature [20-22]. To prepare the decoctions, AR, NR, and AN (3∶1, *W*/*W*) were each mixed with water at a 1∶10 (*W*/*V*) ratio. The mixtures were soaked for 0.5 h, followed by two rounds of decoction, with each session lasting 1 h. After each decoction, the extracts were filtered through eight layers of gauze. The filtered extracts were then concentrated using a rotary evaporator to achieve a final crude drug content of 1.0 g·mL^{-1}. The concentrated liquid was aliquoted and stored at stored in a refrigerator at −20 °C for future use. Additionally, a portion of the concentrated liquid medicine was freeze-dried into powder at −80 °C and preserved in dry form.

2.3. High-performance liquid chromatography-quadrupole-time of flight mass spectrometry/mass spectrometry (HPLC-Q-TOF/MS/MS) analysis

To facilitate further analysis, 1.0 g·mL^{-1} AN extract solution was diluted to 0.5 g·mL^{-1} and subsequently filtered through a 0.22 μm microfiltration membrane. The samples were eluted on a Venusil MP C_{18} column (4.6 mm × 150 mm, 5 μm) and analyzed using an ELSD detector and full wavelength scanning. The mobile phase consisted of acetonitrile (A) and 0.1% formic acid in water (B). Chromatographic separation was conducted at a flow rate of 1 mL·min^{-1}, with the following gradient elution conditions: 5% A (0–1 min), 10% A (1–2 min), 13% A (2–6 min), 19% A (6–10 min), 22% A (10–14 min), 25% A (14–30 min), 62% A (30–46 min), 80% A (46–52 min), 5% A (52–62 min). The column temperature was maintained at 30 °C, and the injection volume was 10 μL.

The electrospray ionization source (ESI) was utilized in both positive and negative ionization modes, with a data acquisition range of 50 to 3000 Da. The MS analysis conditions were established as follows: gas temperature at 325 °C, drying gas flow rate at 9 L·min^{-1}, nebulizer pressure at 35 psi, and capillary voltage at 3.5 kV for the negative mode and 4.0 kV for the positive mode.

2.4. Animals

All procedures involving animals were conducted in accordance with the Guidelines for the Care and Use of Laboratory Animals published by the National Institutes of Health. The experimental protocol was approved by the Animal Ethics Committee of China Pharmaceutical University (Approval No. 220226749). Male Institute of Cancer Research (ICR) mice, 9 weeks old and weighing 22–25 g, were obtained from the Comparative Medical Center of Yangzhou University (Yangzhou, China). Neonatal Sprague-Dawley rats were acquired from Nantong University (Nantong, China). The experimental animal production license numbers were SCXK 2017-0007 and SCXK 2019-0001, respectively. ICR male mice underwent a one-week adaptive housing period, maintained in a stable environment with a 12-h light/dark cycle at 22 ± 2 °C, and provided with adequate food and water.

2.5. Animal model and drug administration

As previously described, the TAC operation induced cardiac hypertrophy in mice [23]. In brief, ICR mice were anesthetized with sodium pentobarbital (30 mg·kg^{-1}) *via* intraperitoneal injection, after which the left chest of each mouse was opened to expose the thoracic aorta. The exposed aorta was then sutured in the thoracic cavity after constriction with 6-0 silk sutures and a 27-gauge needle. Concurrently, sham-operated mice underwent a similar procedure without ligation.

The surviving mice were randomly allocated into seven groups (n = 8–9/group). Two groups of ICR mice underwent sham operation: a sham operation group and a sham operation + AN treatment group (10.4 g·kg^{-1}). Five groups of ICR mice underwent TAC surgery: a TAC group, a TAC + ENP treatment (positive control drug) group (2.6 mg·kg^{-1}), and three TAC + AN treatment groups (2.6, 5.2, and 10.4 g·kg^{-1}). The sham group and TAC group received normal saline. All groups were administered intragastrically at a volume of 10 mL·kg^{-1} once daily for 4 weeks. The ENP dose was based on the clinical dose, while the AN dose was selected according to the Chinese Pharmacopoeia (2020 Edition). The dosage conversion was calculated based on the body surface area between mice and humans.

2.6. Cell isolation and culture

Based on previous research [23, 24], NRCMs and NRCFs were isolated from the cardiac tissue of neonatal Sprague-Dawley rats. Briefly, after heart extraction, ventricular tissues were preserved and minced. The minced tissues were then continuously digested with type II collagenase at 37 °C, and the resulting cell suspension was collected. Leveraging the characteristic that fibroblasts adhere more rapidly than myocardial cells, these two cell types were separated. The adhered NRCFs were cultured in Dulbecco's Modified Eagle Medium (DMEM) supplemented with 10% fetal bovine serum, and second-generation fibroblasts at 80%–90% confluence were used for subsequent experiments. Unattached NRCMs were collected by centrifugation and cultured in DMEM supplemented with 10% fetal bovine serum and 0.1 mmol·L^{-1} 5-bromodeoxyuridine (BrdU) for 48 h before being used in follow-up experiments.

NRCMs and NRCFs were cultured at 37 °C in an incubator with 5% CO_2. An *in vitro* model of myocardial hypertrophy induced by Ang II was established. NRCMs were exposed to 1 μmol·L^{-1} Ang II in DMEM containing 0.5% fetal bovine serum for 48 h, while NRCFs were treated with 1 μmol·L^{-1} Ang II in DMEM without fetal bovine serum for 24 h. Concurrently, AN freeze-dried powder was dissolved in dimethyl sulfoxide (DMSO), and subsequently, NRCMs and NRCFs were treated with AN (12.5, 50, 200 mg·L^{-1}) during Ang II induction.

2.7. Echocardiography analysis

Echocardiography was conducted using the Vevo 3100LT imaging system following four weeks of TAC induction and medical treatment. Mice were anesthetized with 2% isoflurane and secured in a supine position on the ultrasound manipulation panel. The probe position was adjusted based on real-time display images to obtain clear echocardiograms. The following parameters were measured and calculated from the echocardiography: left ventricular ejection fraction (LV EF), left ventricular fractional shortening (LV FS), interventricular septum in diastole (IVS; d), left ventricular mass (LV Mass), and left ventricle volume diastole (LV Vol; d) [25].

2.8. Enzyme-linked immunosorbent assay (ELISA)

Following collection from mice, blood samples were allowed to rest for 60 min. Prior to processing, the centrifuge was pre-cooled to 4 °C. Subsequently, the blood samples were centrifuged at 3500 r·min^{-1} for 10 min, after which the serum was extracted and stored at −80 °C. The serum samples were then processed in accordance with the kit instructions. The absorbance was measured at 450 nm, and the serum levels of IL-6, NT-proBNP, and CTn-T were determined using a standard curve.

2.9. Histopathologic examination

Following euthanasia, the heart tissues of the mice were preserved in a 10% paraformaldehyde solution. The specimens were subsequently embedded in paraffin, sectioned into 5 μm thick slices, and stained with hematoxylin-eosin (H&E) and Masson's trichrome. The sections were then promptly photographed to examine the pathological alterations in the myocardium of the mice. Quantitative analysis of blue collagen deposition was performed using ImageJ software (Bethesda, MD, USA).

2.10. Immunohistochemistry

Heart tissues underwent fixation in paraformaldehyde, followed by paraffin embedding and sectioning into 4–5 μm thick slices. These sections were subsequently dewaxed and treated with 3% hydrogen peroxide. The tissue samples were then incubated with quick-block liquid for 1 h, after which primary antibodies for COL1A1 and COL3A1 were applied and left overnight at 4 °C. Following this, the sections were exposed to HRP-conjugated secondary antibodies for 1 h. Finally, the prepared samples were scanned using a NanoZoom 2.0 RS device (Hamamatsu, Japan).

2.11. Wheat germ agglutinin (WGA) staining

The hearts underwent dehydration using a 40% sucrose solution, followed by embedding in OCT adhesive. Sections of 4–5 μm thickness were obtained using a freezing microtome. The sections were equilibrated at room temperature for 30 min, then incubated with 10 μg·L^{-1} WGA solution for 1 h at room temperature in dark conditions. Subsequently, an anti-fluorescence quenching agent containing DAPI was applied. WGA staining results were observed using a confocal laser scanning microscope (LSM700 Zeiss, Jena, Germany). ImageJ software was utilized to calculate the cross-sectional area of the myocardial cells.

2.12. FITC-labeled phalloidin staining

NRCMs were fixed with 4% paraformaldehyde for 30 min, permeabilized with 0.5% Triton X-100 for 5 min, and blocked with immunostaining rapid blocking solution for 30 min. The samples were then stained with 100 nm FITC-labeled Phalloidin for 30 min at room temperature in darkness, followed by the addition of an anti-fluorescence quencher containing DAPI. Images were acquired using laser confocal microscopy, and the cross-sectional areas of NRCMs were subsequently analyzed using ImageJ software.

2.13. Quantitative real-time PCR (qRT-PCR)

Total RNA was extracted from heart tissues, NRCMs, and NRCFs using a TRIzol reagent (Vazyme, Nanjing, China). RNA concentration and purity were determined by measuring absorption values at 260 and 280 nm using NanoDrop (San Jose, CA, USA). Subsequently, cDNA was synthesized through reverse transcription of RNA following the manufacturer's instructions and added to the qRT-PCR reaction system for amplification. GAPDH served as the reference gene to normalize sample differences, and the relative expression of target genes was calculated using the $2^{-\Delta\Delta CT}$ method. The primer sequences used are detailed in Table 1.

2.14. Western blotting assay

Total protein extraction was performed on heart tissues, NRCMs, and NRCFs. The protein content was measured using the bicinchoninic acid (BCA) protein assay kit to determine the appropriate loading volume. Proteins were separated by sodium dodecyl sulfate-polyacrylamide gel electrophoresis (SDS-PAGE) and subsequently transferred to polyvinylidene fluoride (PVDF) membranes. The membranes were then blocked with 5% bovine serum albumin (BSA) for 2 h at room temperature. Primary antibodies were applied to the membranes and incubated overnight at 4 °C, followed by incubation with secondary antibodies for 1 h at room temperature. All antibodies were diluted according to the manufacturer's instructions. Protein signals were detected using enhanced chemiluminescence (ECL) reagents and quantified using ImageJ software.

2.15. Statistical analysis

Experimental data were presented as mean ± standard devi-

Table 1 The sequences of the primer pairs are as follows.

Genes	Forward	Reverse
Mouse *COL1A1*	CTGACGCATGGCCAAGAAGA	CGTGCCATTGTGGCAGATAC
Mouse *COL3A1*	TGACTGTCCCACGTAAGCAC	GGAGGGCCATAGCTGAACTG
Mouse *ANP*	TCTTCCTCGTCTTGGCCTTT	CCAGGTGGTCTAGCAGGTTC
Mouse *BNP*	TGGGAGGTCACTCCTATCCT	CGTTACAGCCCAAACGACTG
Mouse *MYH7*	CGGACCTTGGAAGACCAGAT	GACAGCTCCCCATTCTCTGT
Mouse *GAPDH*	AACTTTGGCATTGTGGAAGG	ACACATTGGGGGTAGGAACA
Rat *COL1A1*	CGCATGGCCAAGAAGACATC	CTTTGCATAGCACGCCATCG
Rat *COL3A1*	GATGAGCCACTAGACTGCCC	GATAGCCACCCATTCCTCCG
Rat *ANP*	TGGAGCAAATCCCGTATACAGT	TGACCTCATCTTCTACCGGCAT
Rat *BNP*	TCAAAGGACCAAGGCCCTAC	GCCGATCCGGTCTATCTTCTG
Rat *MYH7*	CGGTGACTGTGAAGGAGGAC	TGAGATTGTAGAGCACAGCCG
Rat *GAPDH*	ATGTTCCAGTATGACTC CACTCACG	GAAGACACCAGTAGAC TCCACGACA

ation (SD). Statistical analyses were conducted using GraphPad Prism version 8.0. To evaluate statistical significance among groups, a one-way analysis of variance (ANOVA) was employed. A P value < 0.05 was considered statistically significant.

3. Results

3.1. Component analysis of AN

Employing both positive and negative ion modes of HPLC-Q-TOF-MS/MS and high-performance liquid chromatography, the corresponding signals were analyzed to identify the primary chemical constituents of AN (Fig. S1). By comparing retention behavior with MS data from published literature [26-28], a total of 23 distinct chemical components were identified. Table S1 presents details of the identified compounds.

3.2. AN restored cardiac function in TAC-induced mice

The cardioprotective effect of AN on TAC-induced mice was evaluated through echocardiography. The results revealed significantly lower left ventricular ejection fraction (LV EF) and left ventricular fractional shortening (LV FS) in the model group compared to the sham group (P < 0.01). Additionally, increases in LVS; d, LV Mass, and LV Vol; d were observed (P < 0.01). However, administration of AN at 2.6, 5.2, or 10.4 g·kg^{-1}, as well as ENP treatment, improved these cardiac function indices (Figs. 1A–1F). Further assessment of AN's cardioprotective effect was conducted by measuring serum biochemical indicators. The results demonstrated that AN (10.4 g·kg^{-1}) and ENP treatments effectively reduced serum levels of IL-6, NT-proBNP, and CTn-T in TAC-induced mice (P < 0.01) (Figs. 1G–1I). In conclusion, AN treatment significantly improved cardiac function in TAC-induced mice.

3.3. AN alleviated TAC-induced cardiac hypertrophy

To elucidate the role of AN in TAC-induced cardiac hypertrophy, we observed an enlargement in heart size for TAC-induced mice compared to the sham group. However, TAC-induced mice treated with varying doses of AN and ENP exhibited heart sizes closer to normal (Figs. 2A and 2D). Furthermore, heart weight/body weight ratio (HW/BW) and heart weight/tibia length ratio (HW/TL), both indicators of hypertrophy, were significantly reduced in both AN and ENP administration groups. Additionally, H&E staining results revealed that AN treatment mitigated inflammatory cell infiltration compared to the TAC group. H&E and WGA staining consistently demonstrated that AN and ENP treatments significantly inhibited cardiomyocyte enlargement (P < 0.01) (Figs. 2B, 2C, and 2E). A notable inhibitory effect was observed in the AN administration group (5.2 and 10.4 g·kg^{-1}). Concurrently, we analyzed the expression of hypertrophy-related mRNA, providing further evidence for the anti-myocardial hypertrophy effect of AN. In the TAC-induced group, AN (10.4 g·kg^{-1}) treatment downregulated the expression of *ANP*, *BNP*, and *MYH7* mRNA (P < 0.01) (Figs. 2F–2H). These findings suggest that AN exerts a protective effect against TAC-induced cardiac hypertrophy.

3.4. AN ameliorated TAC-induced cardiac fibrosis

As illustrated in Figs. 3A and 3B, Masson staining revealed increased blue collagen deposition and fibroblast infiltration in the model group, whereas the administration of AN (5.2, 10.4 g·kg^{-1}) and ENP mitigated histopathologic injury and myocardial fibrosis (P < 0.01). Furthermore, immunohistochemistry and qRT-PCR were utilized to assess the expression of fibrosis-related proteins (Figs. 3C–3E). TAC induction significantly elevated COL1A1 and COL3A1 expression compared to the sham group (P < 0.01). However, following AN (10.4 g·kg^{-1}) administration, the expression of COL1A1 and COL3A1 was notably reduced (P < 0.01). Collectively, these results suggest that AN contributed to the amelioration of TAC-induced cardiac fibrosis.

3.5. AN inhibited the activation of the TGF-β1/Smad3 pathway and promoted mitochondrial dynamic balance in vivo

TAC-induced injury activated the TGF-β1/Smad3 pathway and disrupted mitochondrial dynamic balance. The p-Smad3 and TGF-β1 levels were elevated in the model group, while AN (10.4 g·kg^{-1}) treatment inhibited the TGF-β1/Smad3 pathway (Figs. 4A and 4B). Additionally, AN (10.4 g·kg^{-1}) administration increased OPA1 and MFN-2 expression and decreased p-Drp1 expression compared to the TAC group (P < 0.01) (Figs. 4C–4E). Immunohistochemical results further demonstrated that AN administration significantly increased MFN-2 expression and reduced p-Drp1 expression in TAC mice (Fig. 4F). These findings suggest that AN inhibits the TAC-induced activation of the TGF-β1/Smad3 pathway and restores mitochondrial dynamic balance, contributing to the treatment of cardiac remodeling.

3.6. AN mitigated the myocardial hypertrophy and fibrosis in vitro

To further validate the ameliorative effect of AN *in vitro*, NRCMs and NRCFs were treated with Ang II to establish models of cardiomyocyte hypertrophy and fibrosis. Compared to the model group, AN (50, 200 mg·L^{-1}) significantly inhibited the increased cell size in NRCMs (P < 0.01) (Figs. 5A and 5B). Additionally, the mRNA expression levels of *ANP*, *BNP*, and *MYH7* were markedly upregulated upon Ang II induction (P < 0.01), and these changes were reversed after AN treatment (200 mg·L^{-1}) (P < 0.01) (Figs. 5C–5E). Moreover, at the same concentration, AN demonstrated significantly better treatment efficacy compared to AR or NR (Figs. S2A–S2B). Furthermore, AN (50, 200 mg·L^{-1}) treatment

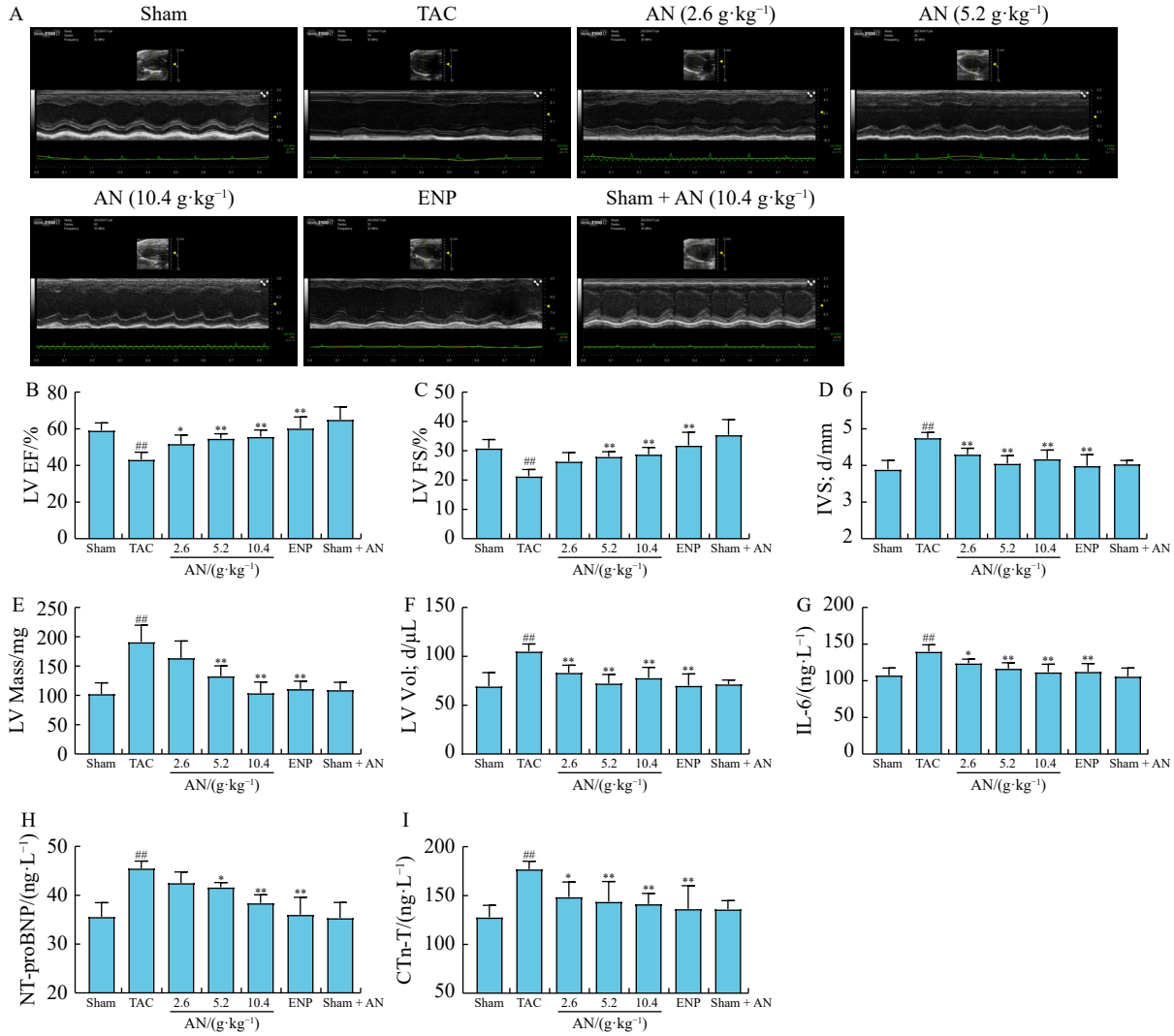

Fig. 1 AN ameliorated cardiac dysfunction in TAC-induced mice. (A) Representative echocardiogram images. (B–F) Statistical analysis of LV EF, LV FS, IVS; d, LV Mass and LV Vol; d following 4 weeks of TAC surgery and treatment in mice (n = 6). (G–I) Quantitative analysis of IL-6, NT-proBNP and CTn-T serum levels (n = 6). Data are presented as mean ± SD. $^{\#}P < 0.05$, $^{\#\#}P < 0.01$ *vs* Sham; $^{*}P < 0.05$, $^{**}P < 0.01$ *vs* TAC.

resulted in reduced levels of *COL1A1* and *COL3A1* mRNA compared to the Ang II group ($P < 0.01$) (Figs. 5F and 5G). Collectively, these *in vitro* findings indicate that AN mitigated Ang II-induced myocardial hypertrophy and fibrosis, consistent with the results obtained *in vivo*.

3.7. AN inhibited activation of TGF-β1/Smad3 pathway and promoted mitochondrial dynamic balance in vitro

As illustrated in Figs. 6A and 6B, p-Smad3 and TGF-β1 expression levels exhibited significant upregulation in Ang II-induced NRCFs, while AN treatment (200 mg·L^{-1}) led to their downregulation. Additionally, Ang II induction resulted in the activation of p-Drp1 levels ($P < 0.05$) and the attenuation of MFN-2 and OPA1 expression in NRCMs. However, administration of AN (200 mg·L^{-1}) reduced p-Drp1 expression ($P < 0.05$) and enhanced the expression of OPA1 and MFN-2 ($P < 0.05$) (Figs. 6C–6E). These findings suggest that AN inhibits the activation of the TGF-β1/Smad3 pathway and promotes mitochondrial dynamic balance *in vitro*, aligning with the aforementioned *in vivo* results.

4. Discussion

Heart failure is primarily a clinical syndrome resulting from impaired systolic or diastolic heart function, secondary to cardiac impairment of diverse etiologies [29, 30]. Pathological cardiac remodeling, a risk factor for heart failure development [31], typically activates signaling pathways, including fibrosis and mitochondrial dysfunction [3]. Consequently, identifying effective treatment methods and therapeutic agents to address pathological cardiac remodeling is crucial. AR–NR, traditional Chinese medicines, are commonly employed in treating various cardiovascular diseases and demonstrate cardioprotective effects [32]. However, research on the mechanism of AN in treating cardiac remodeling is currently limited. Our study elucidates that AN could prevent cardiac remodeling by improving mitochondrial dynamic balance.

Furthermore, the multi-component and synergistic combination of traditional Chinese medicine exerts pharmacological effects through network regulation [33]. In this study, 23 ingredients in the water extract of AN were characterized. Calycosin [34], calycosin-7-*O*-glucoside [35], formononetin [36], and ononin [37] have demonstrated potential to ameliorate atherosclerosis and drug-induced cardiotoxicity. Additionally, notoginsenoside R1 has been shown to alleviate damage caused by myocardial ischemia-reperfusion and promote angiogenesis. These findings suggest that the cardioprotective effect of AN may result from the combined action of the aforementioned components [38, 39]. However, this study has certain limitations. The specific active ingredients in AN that exert therapeutic effects on cardiac remodeling remain unclear, and the interaction of these active ingredients and

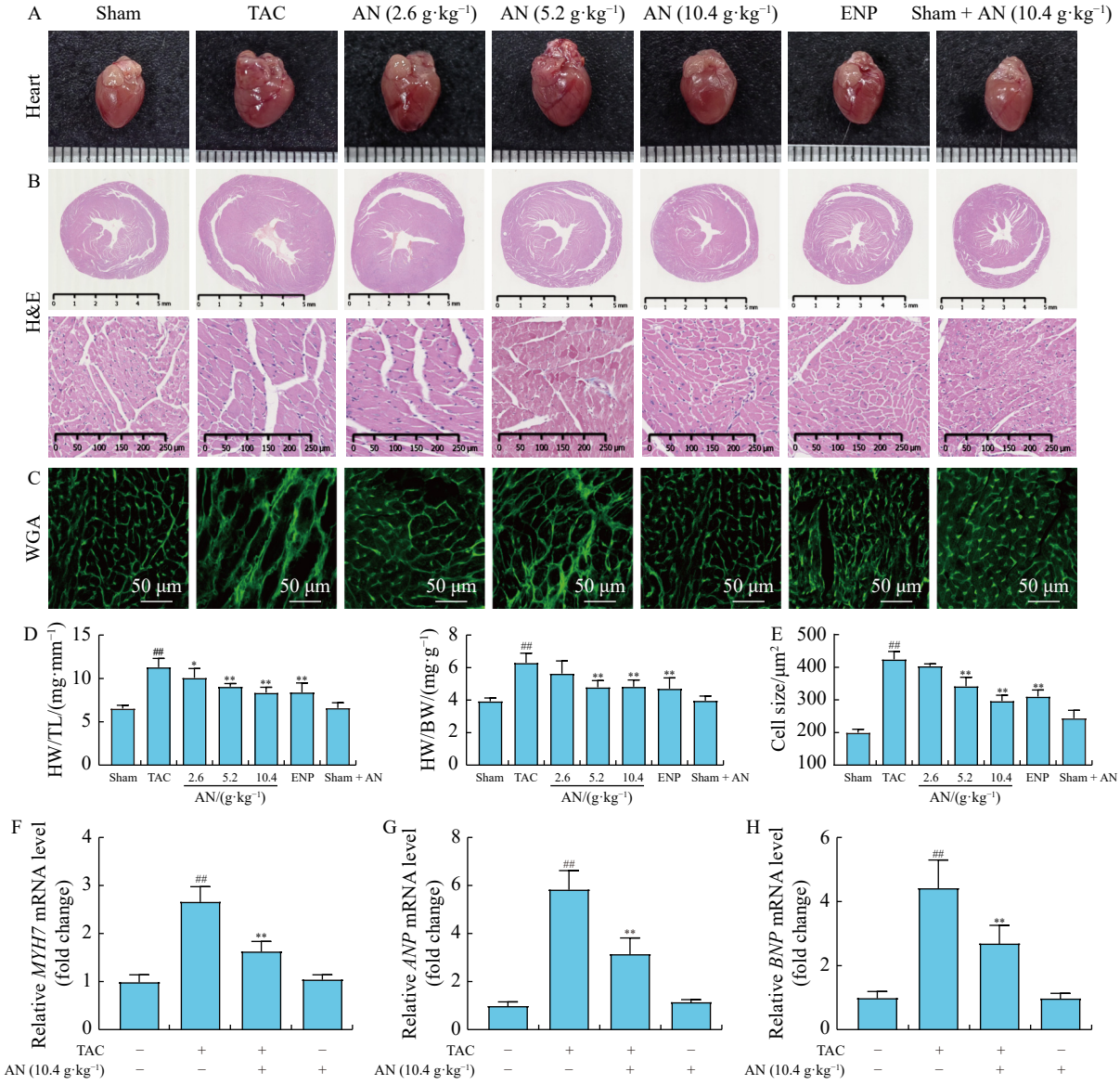

Fig. 2 AN mitigated TAC-induced cardiac hypertrophy. (A) Representative photographs of the whole heart. (B) Representative images of H&E-stained heart tissues (scale bar, 5 mm and 250 μm; $n = 3$). (C) Representative images of WGA-stained heart tissues (scale bar, 50 μm; $n = 3$). (D) The ratios of HW/BW and HW/TL. (E) Statistical analysis of the cross-sectional area of cardiomyocytes ($n = 3$). (F–H) Statistical analyses of *ANP*, *BNP*, and *MYH7* mRNA levels in cardiac tissue after 4 weeks of TAC surgery and treatment ($n = 6$). Results were expressed as mean ± SD. $^{\#}P < 0.05$, $^{\#\#}P < 0.01$ *vs* Sham; $^{*}P < 0.05$, $^{**}P < 0.01$ *vs* TAC.

their potential mechanisms require further investigation.

Cardiac hypertrophy develops gradually through the thickening of the ventricular wall in response to pressure overload or heart damage [40]. Persistent compensatory reactions, however, transition into decompensation and trigger various abnormal signals, including myocardial cell death, fibrosis, mitochondrial dysfunction, and fetal gene re-expression, exacerbating cardiac remodeling and dysfunction [29]. This study employed a TAC-induced cardiac remodeling model that exhibited characteristics consistent with pathological cardiac hypertrophy [41], as evidenced by the increased cross-sectional area of cardiomyocytes and elevated expression of fetal genes (*ANP*, *BNP*, and *MYH7*). Additionally, changes in cardiac function indices such as LV EF, LV FS, LVS; d, LV Mass, and LV Vol; d aligned with previously reported results [23, 41]. Notably, AN significantly reduced serum levels of NT-proBNP, CTn-T, and IL-6 while improving inflammatory cell infiltration, indicating its ameliorative effects on TAC-induced myocardial injury. Furthermore, AN enhanced cardiac function, normalized morphological parameters and sizes of the heart and cardiac myocytes, and inhibited fetal gene expression. *In vitro* experimental data corroborated these observations, demonstrating that AN treatment partially counteracted the adverse effects of Ang II on NRCMs. These findings collectively suggest that AN exhibits favorable therapeutic effects on cardiac hypertrophy and dysfunction.

Pathological cardiac hypertrophy is frequently associated with fibrosis [3]. External pressure stimulation can induce fibroblasts to differentiate into myofibroblast-like phenotypes, resulting in the release of extracellular matrices such as collagen types I and III and TGF-β1 [41]. Collagen type I (Col1), which is more abundant than collagen type III (Col3), determines the mechanical strength of cardiac tissue [42]. Moreover, TGF-β1, a pro-fibrotic cytokine, stimulates Smad3 under pressure load, initiating the progression of cardiac fibrosis [41, 43]. Previous studies have shown that gene deletion of TGF-β1 or Smad3 mitigates pressure overload-induced cardiac fibrosis [44]. In this study, AN decreased collagen deposition, downregulated COL1A1 and COL3A1 expression, and inhibited activation of the TGF-β1/Smad3 pathway in TAC-induced cardiac remodeling. Additionally, these findings were corroborated by our *in vitro* experiments, which demonstrated that AN treatment could partially ameliorate the fibrosis associated with cardiac hypertrophy.

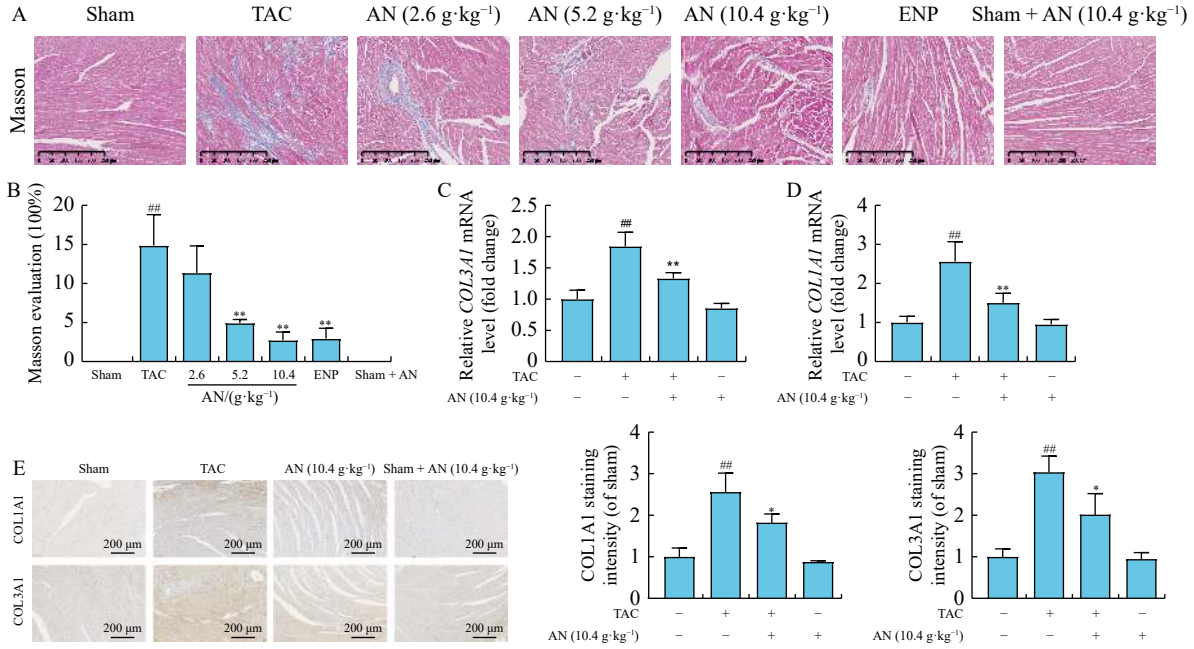

Fig. 3 AN ameliorated TAC-induced cardiac fibrosis. (A, B) Representative images and quantitative analysis of Masson-stained heart tissues (scale bars, 250 μm; $n = 3$). (C, D) Quantitative analysis of *COL1A1* and *COL3A1* mRNA expression in cardiac tissue following 4 weeks of TAC surgery and treatment ($n = 6$). (E) Representative immunohistochemical images and quantitative analysis of COL1A1 and COL3A1 expression in heart tissues after 4 weeks of TAC surgery and treatment (scale bar, 200 μm; $n = 3$). Data are presented as mean ± SD. $^{\#}P < 0.05$, $^{\#\#}P < 0.01$ *vs* Sham; $^{*}P < 0.05$, $^{**}P < 0.01$ *vs* TAC.

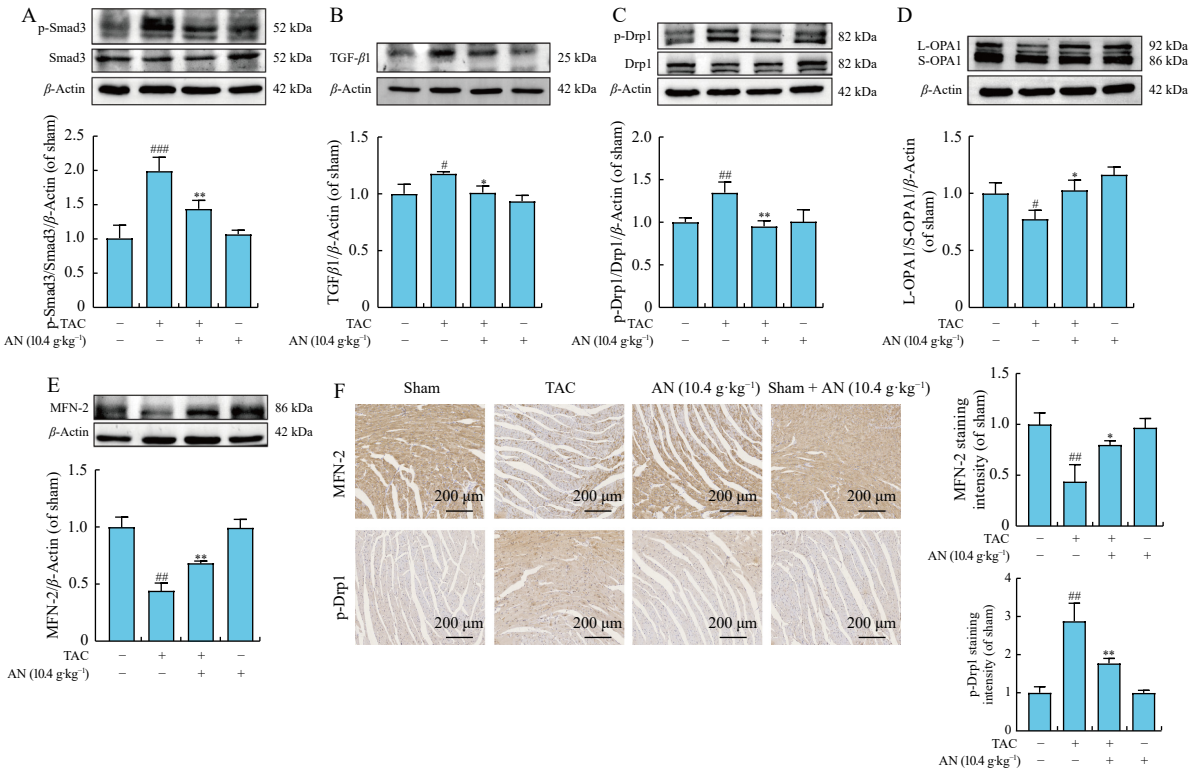

Fig. 4 AN inhibited the activation of TGF-β1/Smad3 pathway and promoted mitochondrial dynamic balance *in vivo*. (A–E) Representative Western blotting images and quantitative analysis of p-Smad3, TGF-β1, p-Drp1, OPA1, and MFN-2 expression in cardiac tissue following 4 weeks of TAC surgery and treatment ($n = 3$). (F) Representative immunohistochemical images and quantitative analysis of MFN-2 and p-Drp1 expression in cardiac tissue after 4 weeks of TAC surgery and treatment (scale bar, 200 μm, $n = 3$). Data are presented as mean ± SD. $^{\#}P < 0.05$, $^{\#\#}P < 0.01$ *vs* Sham; $^{*}P < 0.05$, $^{**}P < 0.01$ *vs* TAC.

Mitochondria, as energy-providing organelles, play a crucial role in maintaining normal cardiac function. Sustaining favorable mitochondrial dynamics is essential for cell survival and functional activities [3]. Drp1 induces mitochondrial division by phosphorylating at serine 616 [45] and recruiting the mitochondrial outer membrane to shrink mitochondria and divide them into two independent organelles. Mitochondrial fusion is mediated by OPA1 and MFN-2 [46]. MFN-2 and OPA1 facilitate the fusion of inner and outer mitochondrial membranes. OPA1 exists in two processed forms: the long form (L-OPA1) is associated with mitochondrial fusion, while the short form (S-OPA1) is related to mitochondrial fission [47]. Furthermore, oligomerized OPA1 regulates

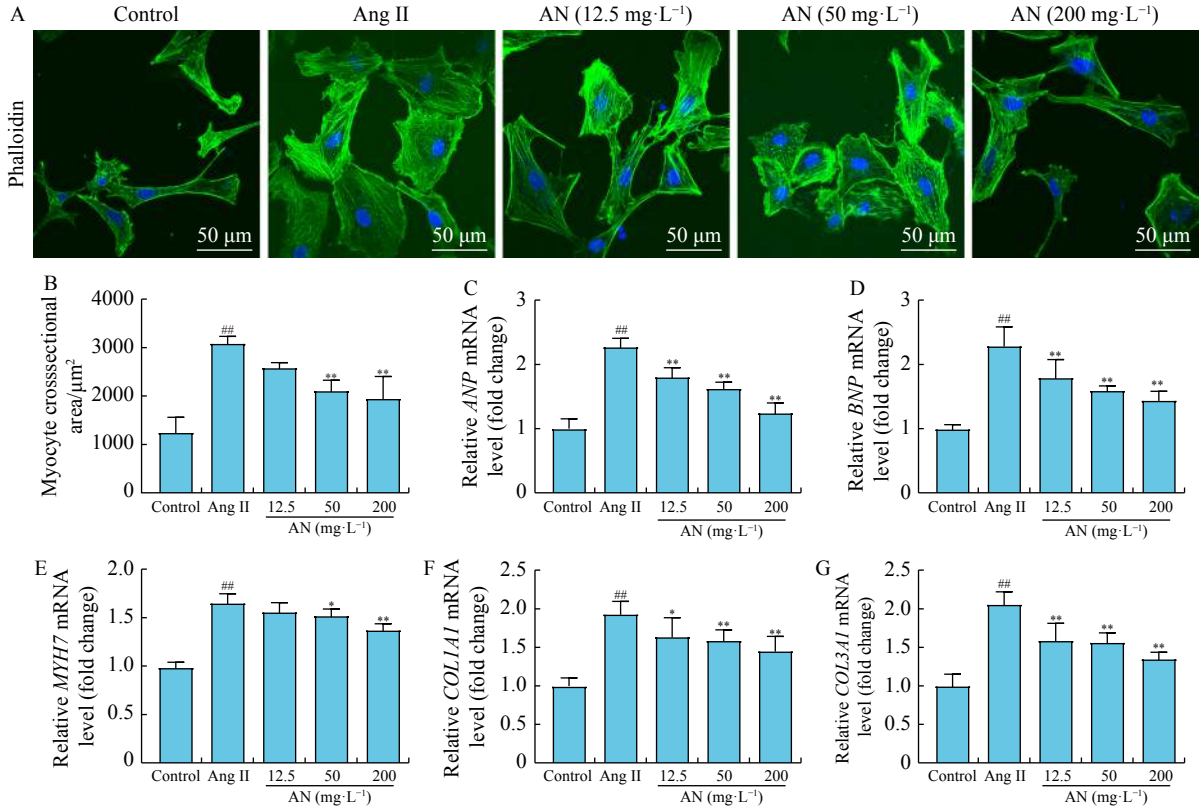

Fig. 5 AN mitigated the myocardial hypertrophy and fibrosis *in vitro*. (A, B) Representative images and statistical analysis of NRCMs stained with FITC-labelled Phalloidin (scale bar, 50 μm; n = 3). (C–G) Statistical analysis of *ANP*, *BNP*, *MYH7*, *COL1A1*, and *COL3A1* mRNA expression levels in NRCMs and NRCFs treated with AN (n = 6). Data are presented as mean ± SD. $^{\#}P < 0.05$, $^{\#\#}P < 0.01$ *vs* Control; $^{*}P < 0.05$, $^{**}P < 0.01$ *vs* Ang II.

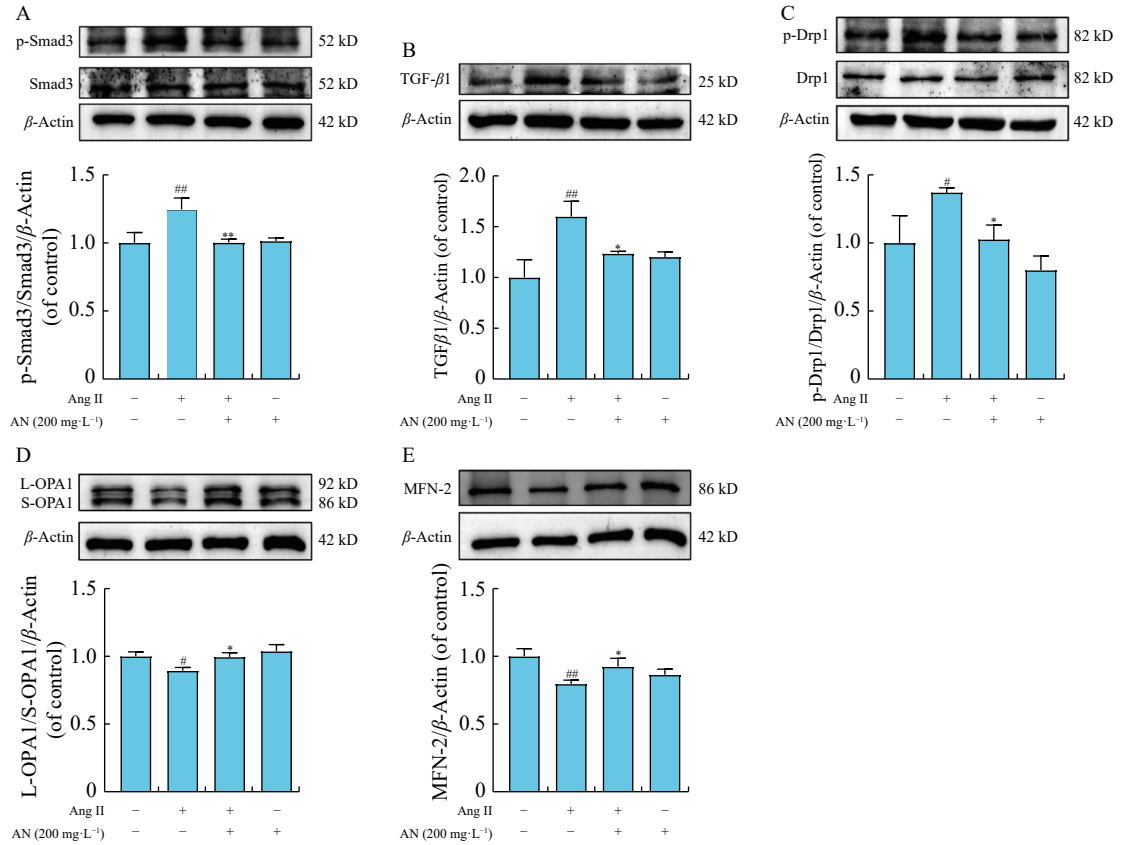

Fig. 6 AN inhibited activation of the TGFβ1/Smad3 pathway and promoted mitochondrial dynamic balance *in vitro*. (A–E) Representative Western blotting images and quantitative analysis of p-Smad3, TGF-β1, p-Drp1, OPA1, and MFN-2 expression in NRCMs and NRCFs treated with AN (n = 3). Data are presented as mean ± SD. $^{\#}P < 0.05$, $^{\#\#}P < 0.01$ *vs* Control; $^{*}P < 0.05$, $^{**}P < 0.01$ *vs* Ang II.

ridge morphology and maintains electron transfer chain operation. Previous studies have shown that inhibiting Drp1 could reduce mitochondrial fission and mitigate myocardial hypertrophy [48, 49]. Additionally, OPA1 and MFN-2 overexpression could enhance mitochondrial fusion and ameliorate myocardial cell damage [50-52]. Consequently, the altered function of proteins involved in mitochondrial fission and fusion can disrupt mitochondrial dynamics, leading to abnormal cardiovascular function. In our study, AN treatment prevented the decrease in OPA1 and MFN-2 levels and the increase in p-Drp1 expression, thereby promoting mitochondrial fusion and inhibiting fission. These findings suggest that AN could improve cardiac remodeling by restoring mitochondrial dynamics balance.

5. Conclusions

This study, employing TAC-induced mice *in vivo* and Ang II-induced NRCMs and NRCFs *in vitro*, elucidated the protective effects of AN on cardiac remodeling through the modulation of mitochondrial dynamics (Fig. 7). Our experimental findings provide a scientific basis for the rational application of traditional Chinese medicine prescriptions primarily composed of AR–NR in clinical practice.

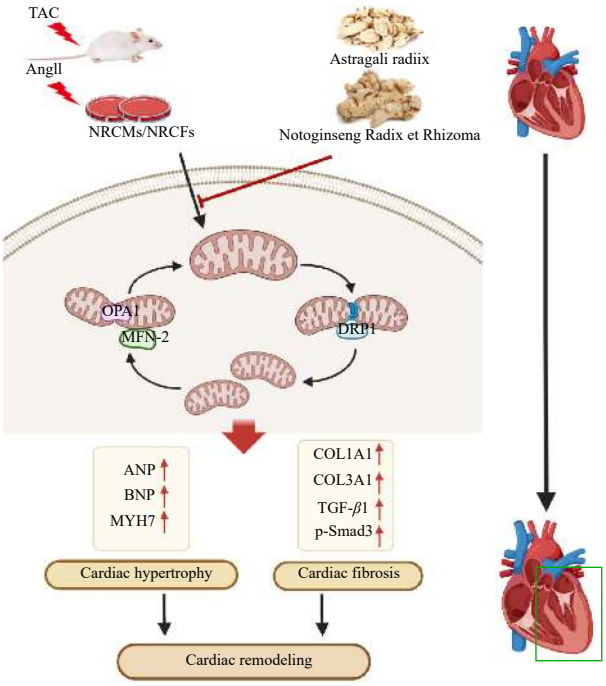

Fig. 7 Schematic diagram of the regulatory mechanism of Astragali Radix–Notoginseng Radix et Rhizoma medicine pair on cardiac remodeling (Created with BioRender.com).

Funding

This research was supported by the National Natural Science Foundation of China (Nos. 82274231 and 81973506), the State Key Laboratory for Chemistry and Molecular Engineering of Medicinal Resources (Guangxi Normal University, No. CMEMR2023-B12), the Fundamental Research Funds for the Central Universities (No. 2632023TD06), the Young Talent Support Project of Jiangsu Association for Science and Technology (No. TJ-2022-025), and the Qinglan Project of Jiangsu Province.

Declaration of competing interest

These authors have no conflict of interest to declare.

Data availability

All data and materials are available can be requested by sending E-mail to the corresponding author.

References

1 Bragazzi NL, Zhong W, Shu J, et al. Burden of heart failure and underlying causes in 195 countries and territories from 1990 to 2017. *Eur J Prev Cardiol*. 2021;28(15):1682–1690. https://doi.org/10.1093/eurjpc/zwaa147.
2 Forte M, Schirone L, Ameri P, et al. The role of mitochondrial dynamics in cardiovascular diseases. *Br J Pharmacol*. 2020;178(10):2060–2076. https://doi.org/10.1111/bph.15068.
3 Nakamura M, Sadoshima J. Mechanisms of physiological and pathological cardiac hypertrophy. *Nat Rev Cardiol*. 2018;15(7):387–407. https://doi.org/10.1038/s41569-018-0007-y.
4 Winkle AJ, Nassal DM, Shaheen R, et al. Emerging therapeutic targets for cardiac hypertrophy. *Expert Opin Ther Targets*. 2022;26(1):29–40. https://doi.org/10.1080/14728222.2022.2031974.
5 Zhou B, Tian R. Mitochondrial dysfunction in pathophysiology of heart failure. *J Clin Invest*. 2018;128(9):3716–3726. https://doi.org/10.1172/JCI120849.
6 Jin JY, Wei XX, Zhi XL, et al. Drp1-dependent mitochondrial fission in cardiovascular disease. *Acta Pharmacol Sin*. 2020;42(5):655–664. https://doi.org/10.1038/s41401-020-00518-y.
7 Jhun B, O-Uchi J, Adaniya S, et al. Adrenergic regulation of drp1-driven mitochondrial fission in cardiac physio-pathology. *Antioxidants (Basel)*. 2018;7(12):195. https://doi.org/10.3390/antiox7120195.
8 Hasan P, Saotome M, Ikoma T, et al. Mitochondrial fission protein, dynamin-related protein 1, contributes to the promotion of hypertensive cardiac hypertrophy and fibrosis in Dahl-salt sensitive rats. *J Mol Cell Cardiol*. 2018;121:103–106. https://doi.org/10.1016/j.yjmcc.2018.07.004.
9 Shirakabe A, Zhai P, Ikeda Y, et al. Drp1-dependent mitochondrial autophagy plays a protective role against pressure overload-induced mitochondrial dysfunction and heart failure. *Circulation*. 2016;133(13):1249–1263. https://doi.org/10.1161/CIRCULATIONAHA.115.020502.
10 Meng G, Liu J, Liu S, et al. Hydrogen sulfide pretreatment improves mitochondrial function in myocardial hypertrophy *via* a SIRT3-dependent manner. *Br J Pharmacol*. 2017;175(8):1126–1145. https://doi.org/10.1111/bph.13861.
11 Dong PL, Li H, Yu XJ, et al. Effect and mechanism of "Danggui-Kushen" herb pair on ischemic heart disease. *Biomed Pharmacother*. 2022;145:112450. https://doi.org/10.1016/j.biopha.2021.112450.
12 Zhang JX, Hu DJ, Du W, et al. Effects of *Astragalus* extract on serum cTnI and TGF-β1 in rats with myocardial infarction. *Hebei Med J*. 2020;42(10):1475–1478. https://doi.org/10.3969/j.issn.1002-7386.2020.10.007.
13 Ma X, Zhang K, Li H, et al. Extracts from *Astragalus membranaceus* limit myocardial cell death and improve cardiac function in a rat model of myocardial ischemia. *J Ethnopharmacol*. 2013;149(3):720–728. https://doi.org/10.1016/j.jep.2013.07.036.
14 Cheng L, Wang Q, Meng G, et al. Effect of *Astragalus* extract on oxidative stress and cardiac function protection on rat models with viral myocarditis infection. *Chin J Nosocomiol*. 2023;33(10):1463–1467. https://doi.org/10.11816/cn.ni.2023-221289.
15 Wang LC, Zhang WS, Liu Q, et al. A standardized *Notoginseng* extract exerts cardioprotection by attenuating apoptosis under endoplasmic reticulum stress conditions. *J Funct Foods*. 2015;16:20–27. https://doi.org/10.1016/j.jff.2015.04.018.
16 Han SY, Li HX, Ma X, et al. Evaluation of the anti-myocardial ischemia effect of individual and combined extracts of *Panax notoginseng* and *Carthamus tinctorius* in rats. *J Ethnopharmacol*. 2013;145(3):722–727. https://doi.org/10.1016/j.jep.2012.11.036.
17 Loh YC, Tan CS, Ch'ng YS, et al. Mechanisms of action of *Panax notoginseng* ethanolic extract for its vasodilatory effects and partial characterization of vasoactive compounds. *Hypertens Res*. 2018;42(2):182–194. https://doi.org/10.1038/s41440-018-0139-9.
18 Zhang WQ, Zhang ZL, Zhang N, et al. Comparative study on the active components and efficacy of *Astragalus membranaceus* (Fisch.) Bunge and *Panax Notoginseng* compound by two different preparation methods. *Prog Mod Biomed*. 2023;23(24):4607–4613. https://doi.org/10.13241/j.cnki.pmb.2023.24.002.
19 Lu JQ, Lin H, Zhu ZD, et al. Advances in research on the effects of regulating lipid metabolism using *Astragalus mongholicus* and pseudo-ginseng on MACE and analysis of potential mechanisms. *Chin Gen Pract*. 2020;23(27):3466–3473. https://doi.org/10.12114/j.issn.1007-9572.2020.00.308.
20 Shi P, Chai XQ, Lei B, et al. Clinical observation of Huangqi Sanqi Powder in promoting wound healing of 60 cases of anal fistula. *Clin Res Pract*. 2018;3(11):114–115. https://doi.org/10.19347/j.cnki.2096-1413.201811054.
21 Lei, XQ, Wei HY, Tan RZ, et al. Effects of Huangqi Sanqi Mixture on cisplatin-induced acute kidney injury in mice. *Chin Tradit Pat Med*. 2022;44(04):1107–1113. https://doi.org/10.3969/j.issn.1001-1528.2022.04.012.
22 Xu, SS, Wang BG, Liu XC, et al. Mechanism study on herbal pair of Radix Astragali and Radix Notoginseng for alleviating cerebral ischemia-reperfusion injury in rats *via* inhibiting inflammatory cascade reaction. *J Guangzhou Univ of Tradit Chin Med*. 2021;38(3):576–582. https://doi.org/10.13359/j.cnki.gzxbtcm.2021.03.025.
23 Chen QQ, Ma G, Liu JF, et al. Neuraminidase 1 is a driver of experimental cardiac hypertrophy. *Eur Heart J*. 2021;42(36):3770–3782. https://doi.org/10.1093/eurheartj/ehab347.

24 Maass AH, Buvoli M. Cardiomyocyte preparation, culture, and gene transfer. *Methods Mol Biol*. 2007;366:321–330. https://doi.org/10.1007/978-1-59745-030-0_18.

25 Gjesdal O, Bluemke DA, Lima JA. Cardiac remodeling at the population level-risk factors, screening, and outcomes. *Nat Rev Cardiol*. 2011;8(12):673–685. https://doi.org/10.1038/nrcardio.2011.154.

26 Liu P, Yu HS, Zhang LJ, et al. A rapid method for chemical fingerprint analysis of *Panax notoginseng* powders by ultra performance liquid chromatography coupled with quadrupole time-of-flight mass spectrometry. *Chin J Nat Med*. 2015;13(6):471–480. https://doi.org/10.1016/S1875-5364(15)30042-X.

27 Liang C, Yao Y, Ding H, et al. Rapid classification and identification of chemical components of Astragali Radix by UPLC-Q-TOF-MS. *Phytochem Anal*. 2022;33(6):943–960. https://doi.org/10.1002/pca.3150.

28 Li Y, Huang S, Sun J, et al. RRLC-QTOF/MS-based metabolomics reveal the mechanism of chemical variations and transformations of Astragali Radix as a result of the roasting process. *Front Chem*. 2022;10:903168. https://doi.org/10.3389/fchem.2022.903168.

29 Ziaeian B, Fonarow GC. Epidemiology and aetiology of heart failure. *Nat Rev Cardiol*. 2016;13(6):368–378. https://doi.org/10.1038/nrcardio.2016.25.

30 Savarese G, Becher PM, Lund LH, et al. Global burden of heart failure: a comprehensive and updated review of epidemiology. *Cardiovasc Res*. 2022;118(17):3272–3287. https://doi.org/10.1093/cvr/cvac013.

31 Reid BG, Stratton MS, Bowers S, et al. Discovery of novel small molecule inhibitors of cardiac hypertrophy using high throughput, high content imaging. *J Mol Cell Cardiol*. 2016;97:106–113. https://doi.org/10.1016/j.yjmcc.2016.04.015.

32 Gao J, Lyu M, Xie WW, et al. Regularity of traditional Chinese medicine prescriptions for same treatment for cardiovascular and cerebrovascular diseases. *Chin J Chin Mater Med*. 2019;44(1):193–198. https://doi.org/10.19540/j.cnki.cjcmm.20181101.007.

33 Yang HY, Liu ML, Luo P, et al. Network pharmacology provides a systematic approach to understanding the treatment of ischemic heart diseases with traditional Chinese medicine. *Phytomedicine*. 2022;104:154268. https://doi.org/10.1016/j.phymed.2022.154268.

34 Ding WJ, Chen GH, Deng SH, et al. Calycosin protects against oxidative stress-induced cardiomyocyte apoptosis by activating aldehyde dehydrogenase 2. *Phytother Res*. 2023;37(1):35–49. https://doi.org/10.1002/ptr.7591.

35 Yan X, Yu A, Zheng H, et al. Calycosin-7-*O*-*β*-D-glucoside attenuates OGD/R-induced damage by preventing oxidative stress and neuronal apoptosis *via* the SIRT1/FOXO1/PGC-1α pathway in HT22 cells. *Neural Plast*. 2019;2019:8798069. https://doi.org/10.1155/2019/8798069.

36 Ma C, Xia R, Yang S, et al. Formononetin attenuates atherosclerosis *via* regulating interaction between KLF4 and SRA in apoE$^{-/-}$ mice. *Theranostics*. 2020;10(3):1090–1106. https://doi.org/10.7150/thno.38115.

37 Pan R, Zhuang Q, Wang J. Ononin alleviates H_2O_2-induced cardiomyocyte apoptosis and improves cardiac function by activating the AMPK/mTOR/autophagy pathway. *Exp Ther Med*. 2021;22(5):1307. https://doi.org/10.3892/etm.2021.10742.

38 Zeng JJ, Shi HQ, Ren FF, et al. Notoginsenoside R1 protects against myocardial ischemia/reperfusion injury in mice *via* suppressing TAK1-JNK/p38 signaling. *Acta Pharmacol Sin*. 2023;44(7):1366–1379. https://doi.org/10.1038/s41401-023-01057-y.

39 Zhong J, Lu W, Zhang J, et al. Notoginsenoside R1 activates the Ang2/Tie2 pathway to promote angiogenesis. *Phytomedicine*. 2020;78:153302. https://doi.org/10.1016/j.phymed.2020.153302.

40 Wu QQ, Xiao Y, Yuan Y, et al. Mechanisms contributing to cardiac remodelling. *Clin Sci (Lond)*. 2017;131(18):2319–2345. https://doi.org/10.1042/CS20171167.

41 Bazgir F, Nau J, Nakhaei-Rad S, et al. The microenvironment of the pathogenesis of cardiac hypertrophy. *Cells*. 2023;12(13):1780. https://doi.org/10.3390/cells12131780.

42 Worke LJ, Barthold JE, Seelbinder B, et al. Densification of type I collagen matrices as a model for cardiac fibrosis. *Adv Healthc Mater*. 2017;6(22):10. https://doi.org/10.1002/adhm.201700114.

43 Zeng Z, Wang Q, Yang X, et al. Qishen Granule attenuates cardiac fibrosis by regulating TGF-β /Smad3 and GSK-3β pathway. *Phytomedicine*. 2019;62:152949. https://doi.org/10.1016/j.phymed.2019.152949.

44 Khalil H, Kanisicak O, Prasad V, et al. Fibroblast-specific TGF-β-Smad2/3 signaling underlies cardiac fibrosis. *J Clin Invest*. 2017;127(10):3770–3783. https://doi.org/10.1172/JCI94753.

45 Garone C, Minczuk M, Tilokani L, et al. Mitochondrial dynamics: overview of molecular mechanisms. *Essays Biochem*. 2018;62(3):341–360. https://doi.org/10.1042/EBC20170104.

46 Adebayo M, Singh S, Singh AP, et al. Mitochondrial fusion and fission: the fine-tune balance for cellular homeostasis. *FASEB J*. 2021;35(6):e21620. https://doi.org/10.1096/fj.202100067R.

47 Zhuang Q, Guo F, Fu L, et al. 1-Deoxynojirimycin promotes cardiac function and rescues mitochondrial cristae in mitochondrial hypertrophic cardiomyopathy. *J Clin Invest*. 2023;133(14):e164660. https://doi.org/10.1172/JCI164660.

48 Hu Q, Zhang H, Gutiérrez CN, et al. Increased Drp1 acetylation by lipid overload induces cardiomyocyte death and heart dysfunction. *Circulation Res*. 2020;126(4):456–470. https://doi.org/10.1161/CIRCRESAHA.119.315252.

49 Wu QR, Zheng DL, Liu PM, et al. High glucose induces Drp1-mediated mitochondrial fission *via* the orai1 calcium channel to participate in diabetic cardiomyocyte hypertrophy. *Cell Death Dis*. 2021;12(2):216. https://doi.org/10.1038/s41419-021-03502-4.

50 Xiong W, Ma Z, An D, et al. Mitofusin 2 participates in mitophagy and mitochondrial fusion against angiotensin II-induced cardiomyocyte injury. *Front Physiol*. 2019;10:411. https://doi.org/10.3389/fphys.2019.00411.

51 Ma Z, Liu Z, Li X, et al. Metformin collaborates with PINK1/Mfn2 overexpression to prevent cardiac injury by improving mitochondrial function. *Biology (Basel)*. 2023;12(4):582. https://doi.org/10.3390/biology12040582.

52 Luo F, Fu M, Wang T, et al. Down-regulation of the mitochondrial fusion protein Opa1/Mfn2 promotes cardiomyocyte hypertrophy in Su5416/hypoxia-induced pulmonary hypertension rats. *Arch Biochem Biophys*. 2023;747:109743. https://doi.org/10.1016/j.abb.2023.109743.